Computational Materials Science 48 (2010) 426–439

Contents lists available at ScienceDirect

Computational Materials Science

journal homepage: www.elsevier.com/locate/commatsci

Fatigue crack growth in magnesium single crystals under cyclic loading: Molecular dynamics simulation

Tian Tang *, Sungho Kim, M.F. Horstemeyer

Center for Advanced Vehicular System, Mississippi State University, Box 5405, Mississippi State, MS 39762, USA

ARTICLE INFO

Article history:
Received 14 September 2009
Received in revised form 19 January 2010
Accepted 2 February 2010
Available online 2 March 2010

Keywords:
Molecular dynamics simulation
Fatigue crack propagation
Magnesium single crystal
EAM
Crystal orientation

ABSTRACT

The fatigue crack propagation behavior of magnesium single crystal was analyzed using molecular dynamics simulation. The inter-atomic potential used in this investigation is Embedded Atom Method (EAM) potentials. The studies of the mechanism of fatigue crack growth in different crystal orientation were performed using Center Crack (CC) specimens while Edge Crack (EC) specimens were employed to investigate the effects of strain rate and temperature. For CC specimen, the periodic boundary conditions were assigned in the *x* and *z* direction, while for EC specimen, only *z* direction was allowed periodic boundary conditions. In order to study the orientation dependence of fatigue crack growth mechanism, 10 crystal orientations of initial crack were analyzed and the simulation results reveal that the fatigue crack growth rate and the crack path vary significantly with the crystallographic orientations of initial crack. The growth rate of orientation D is the highest and the resistance of fatigue crack growth of orientation B is the highest. The analysis of the influences of strain rate was carried out on the orientation F and the results revealed that the growth rate of fatigue crack decreasing with increasing strain rate. The fatigue crack growth rates of different orientation decrease with increasing temperature.

Published by Elsevier B.V.

1. Introduction

Magnesium has a hexagonal close-packed (HCP) crystal structure which present unique feature not encountered in cubic structures. In recent years, the application of magnesium alloys to lightweight structural component in aerospace and vehicles has significantly increased due to their low density, excellent castability, and high strength-to-weight ratio [1–6]. Therefore, it is important to get better understanding of its fatigue crack growth behavior.

Many research efforts have been devoted to the investigation of fatigue crack propagation behavior in bcc and fcc metals, while the experimental studies of fatigue crack behavior in magnesium single crystal were performed only by several researchers [7] who clarified the orientation dependence of fatigue crack propagation mechanisms. So far the researches are limited to meso/macro scale. Along with the developments of nanomaterials, it is absolutely necessary to extend the studies into the atomic scale. Meanwhile, the investigation of mechanical properties of metal at atomic scale is an important multi-scale engineering effort. On the contrary to continuum theories, molecular dynamics (MD) is capable of providing atomic description of fatigue problems. As long as the inter-atomic potential is reliable, it can disclose the fundamental physical mechanism of fatigue. To the best of the author's knowledge, only several researchers utilized molecular dynamics to simulate the fatigue crack propagation behavior in face-centered cubic copper and nickel [8–11], they concluded that the cyclic plastic deformation around crack tip and the resulting nanovoids nucleation in front of the crack tip is the main mechanism for the propagation of nanocrack. Nishimura and Miyazaki [12] used MD to study the fatigue crack growth in a system containing both a crack and two tilt grain boundaries. Their simulation results reveal that the mechanism of fatigue crack propagation is due to the coalescence of the crack and the vacancies caused by the emission and absorption of dislocations. Generally speaking, all investigations on bcc and fcc metals indicated that the essence of fatigue crack growth is the plastic deformation around the crack tip. Almost no atomistic modeling, however, has been performed on HCP metals.

In some cases, operating temperatures for structural components have increased for better thermal efficiency. Therefore, the temperature effects on fatigue have been an important research topic. Lim et al. [13] experimentally studied the effect of temperature on fatigue crack growth in P92 steel. They concluded that the Paris exponent remained at approximately the same value up to a certain temperature. Chang and Fang [14] investigated the influences of temperature on tensile and fatigue behavior of nanoscale copper using molecular dynamics simulation. The simulation results reveal that the fatigue stress increased with increasing temperature.

* Corresponding author. Tel.: +1 662 3259222.
E-mail address: tian.tang@aggiemail.usu.edu (T. Tang).

0927-0256/$ - see front matter Published by Elsevier B.V.
doi:10.1016/j.commatsci.2010.02.003

On the other hand, extensive researches have been carried out on the temperature effects on fatigue of polymers [15].

In the present paper, we analyze the fatigue behavior in magnesium single crystal using molecular dynamics simulation. Our goals are to reveal the influences of lattice orientation, strain rate, and temperature. The development of dislocation and twin structure around crack tip is also displayed by simulation. The detailed twin nucleation mechanism at crack tip will be a significant future study.

2. Simulation method

The inter-atomic potential used in this study is an Embedded Atom Method (EAM) potential developed by Sun et al. [16]. This form of EAM consists of two contributions to the total potential energy, E, of the entire system composed of N atoms. The functional form of the total embedded energy can be expressed as

$$E = \sum_i G_i\left(\sum_{j\neq i} \rho_j^a(r_{ij})\right) + \frac{1}{2}\sum_{ij} U_{ij}(r_{ij}) \tag{1}$$

where G_i is the embedding energy as a function of the local electron density, ρ_j^a is the spherically averaged atomic electron density, U_{ij} is the pair potential, and r_{ij} is the distance between atom i and j. Many examples have demonstrated that EAM can be an accurate representation of inter-atomic forces in a metallic lattice. In molecular dynamics, the energy is employed to determine the forces acting on each atom. At each atom the dipole force tensor β_{ij}, is given by

$$\beta_{km}^i = \frac{1}{\Omega^i}\sum_{j(\neq i)}^{N} f_k^i(r^{ij}) r_m^{ij} \tag{2}$$

where f_k is the force vector between atoms, r_m is the displacement vector between atoms i and j, N is the number of nearest neighbor atoms, and Ω^i is the atomic volume. If stress could be defined at an atom, then β_{ij} would be the stress tensor at that point. Since stress is defined at a continuum point, the stress tensor can be determined as a volume average over the block of material,

$$\sigma_{mk} = \frac{1}{N^*}\sum_i^{N^*} \beta_{mk}^i \tag{3}$$

in which the stress tensor is defined in terms of the total number of atoms, N^*, in the block of material. The averaged stresses are used to determine the uniaxial stress–strain response.

3. Atomistic model and crystal orientation

To investigate the fatigue crack growth, we used two types of specimens, namely, Center Crack (CC) and Edge Crack (EC) specimens as indicated in Figs. 1 and 2, respectively. In both specimens, the initial cracks were introduced by removing the atoms from the perfect crystals. The ratio of the initial crack length to the width of the specimen was $a_0/w = 1/15$ for CC specimen but $a_0/w = 0.2$ for EC specimen. For each type of specimen, 10 different crystal orientations of initial crack, namely, orientation A-$(1\,\bar{2}\,1\,0)[1\,0\,\bar{1}\,0]$, orientation B-$(10\,\bar{1}\,0)[1\,\bar{2}\,10]$, orientation C-$(1\,0\,\bar{1}\,0)[0\,0\,0\,1]$, orientation D-$(1\,\bar{2}\,1\,0)[0\,0\,0\,1]$, orientation E-$(0\,0\,0\,1)[1\,0\bar{1}\,0]$, orientation F-$(0\,0\,0\,1)[1\,\bar{2}\,1\,0]$, orientation G-$(1\,0\,\bar{1}\,1)[1\,0\,1\,2]$, orientation H-$(1\,0\,\bar{2}\,1)[1\,\bar{2}\,1\,0]$, orientation I-$(1\,0\,\bar{1}\,2)[1\,0\,\bar{1}\,1]$, and orientation J-$(1\,0\,\bar{1}\,2)[1\,\bar{2}\,1\,0]$, were considered and illustrated in Fig. 3. These orientations represent all of the possible orientation of interest in HCP structure. A summary of the dimensions of different crystal orientation and the resulting number of atoms of CC and EC specimen were presented in Tables 1 and 2, respectively. In both specimens, the cyclic loading is applied along y direction which is perpendicular to the crack plane. The periodic boundary condition is assigned in the x and z directions in CC specimen while, in EC specimen, only the x direction was assigned periodic boundary condition. The x axis represents the direction of crack extension while the z represents the direction of thickness. These models are initially free of dislocations and twin.

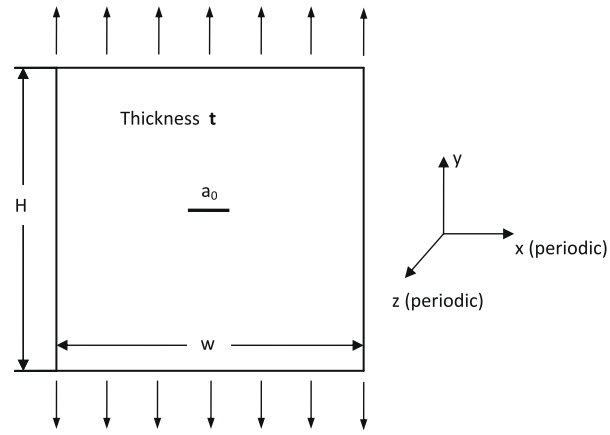

Fig. 1. CC specimen used for the simulation of fatigue crack growth.

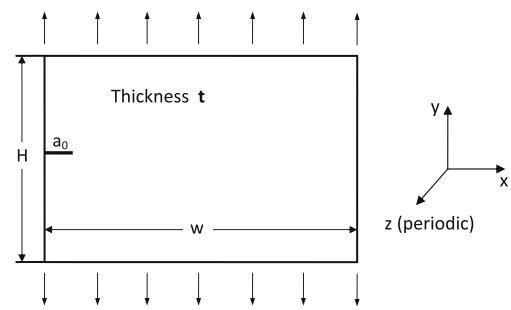

Fig. 2. EC specimen used for the simulation of fatigue crack growth.

4. Lattice constants

To study the temperature effects on fatigue crack propagation, we calculate the lattice constants of magnesium at various temperatures. In this calculation, we create a three dimensional model without defects. Periodic boundary conditions are assigned to all of three directions. The thermal expansion of the model is isotropic. This model was firstly equilibrated at constant temperature and zero pressure. The temperature was controlled by rescaling the velocities of atoms while the pressure of the model was set to zero by using a Berendsen barostat. Finally, the group of atoms were performed constant NPT integration to update positions and velocities each timestep. P is pressure; T is temperature. This creates a system trajectory consistent with the isothermal–isobaric ensemble. The variation of lattice constants c and a with temperature are plotted in Fig. 4.

5. Simulation results and discussions

In this section, we presented the illustrative results of molecular dynamics for clarifying the effects of crystal orientation, strain rate, and temperature on the fatigue crack propagation in magnesium single crystal. In some cases, the fatigue damage caused by increasing maximum strain was also discussed. The centrosymmetry

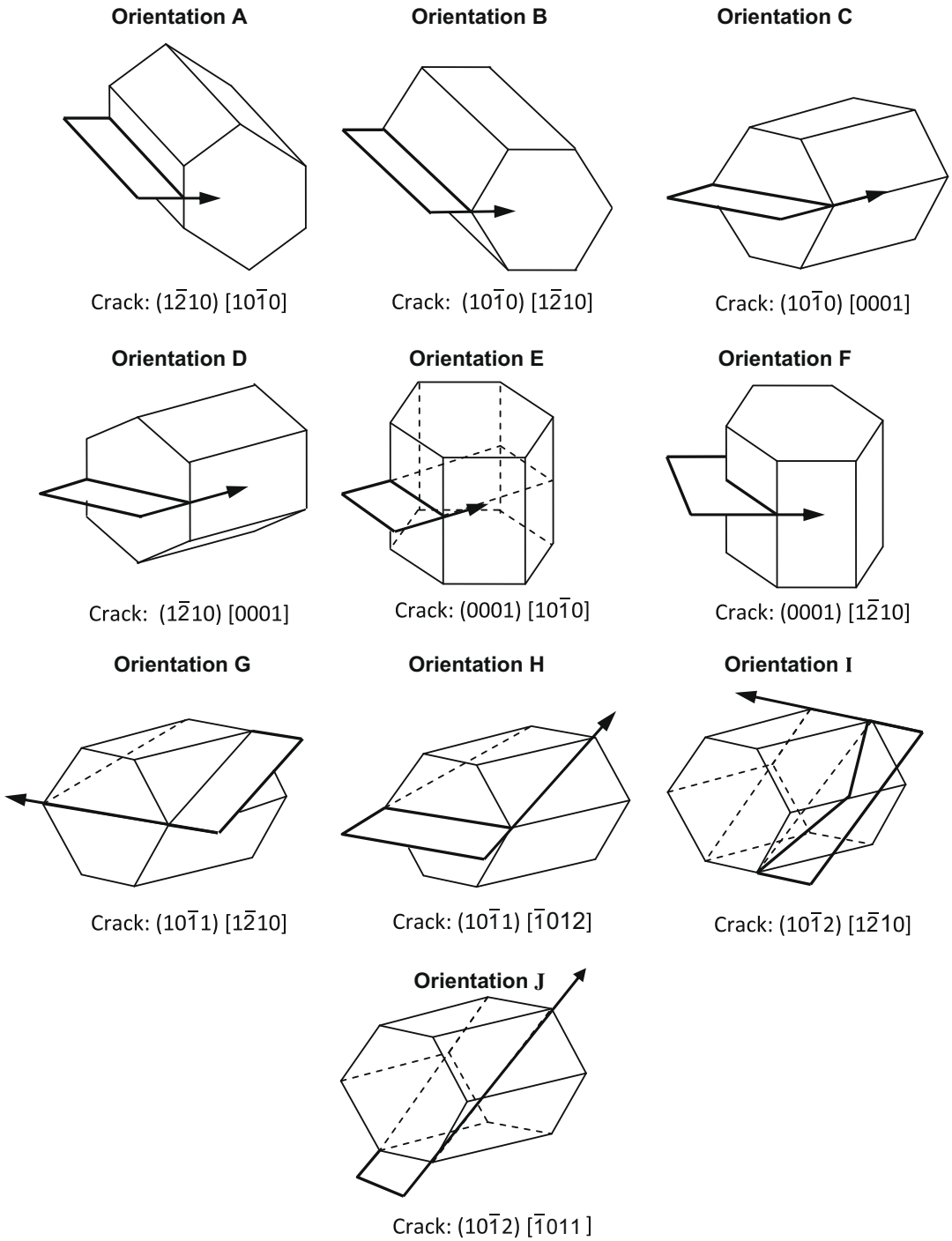

Fig. 3. Crystallographic orientations of the initial cracks.

parameter defined by Kelchner et al. [17] was used to highlight the defects including crack surface, slip band, and twin. The expression of this parameter is given by

$$P = \sum_i |R_i + R_{i+6}|^2 \tag{4}$$

where R_i and R_{i+6} are the vectors or bonds corresponding to the six pairs out of 12 nearest neighbors in the lattice. The six pairs are chosen to minimize P. The P values for the atoms in fcc and hcp structures, dislocations, twinning boundaries and crack surfaces are all different so that extensive information about crack growth and many defect behaviors can be obtained.

5.1. Fatigue crack growth in single crystal

Firstly, CC specimens were used to investigate the effects of orientation of initial crack on the mechanism of fatigue crack growth. In order to determine the critical value of maximum tension strain at which the fatigue crack start growing, we performed a monotonic tension test. Each specimen was subjected to uniaxial tension with strain rate $1.5 \times 10^9\ s^{-1}$ until the initial crack started growing. The simulations were carried out at a constant temperature of 100 K. Table 3 present the critical values of maximum tension strain ε_{cri} for orientation A–J obtained from monotonic tension test. It can be seen that the critical values of ε_{max} vary widely with crys-

Table 1
Summary of the dimension and number of atoms in the Center Crack (CC) specimen for orientation A–J.

Orientations	H (nm)	W (nm)	t (nm)	Number of atoms
A	48	40	2.082	170,364
B	69.2	40	2.085	249,964
C	40	40	1.280	89,912
D	40	40	2.216	153,956
E	40	40	1.280	89,896
F	40	40	2.216	153,932
G	40	40	1.180	81,468
H	40	40	1.120	88,636
I	40	40	1.520	105,468
J	40	40	1.280	89,436

Table 2
Summary of the dimension and number of atoms in the Edge Crack (EC) specimen for orientation A–J.

Orientations	H (nm)	W (nm)	t (nm)	Number of atoms
A	36	50	2.074	164,084
B	36	50	2.074	162,904
C	36	50	1.280	99,608
D	36	50	2.206	173,100
E	36	50	1.280	100,316
F	36	50	2.206	173,076
G	36	50	2.36	185,392
H	36	50	2.56	203,104
I	36	50	2.28	179,550
J	36	50	2.56	201,272

tallographic orientation of the initial cracks. In the case of orientation B, the critical value of ε_{cri} was not available since the crack was blunted seriously and did not grow even though the applied tension strain was very high. However, the crack started growing along the slip band on the $(1\ 0\ \bar{1}\ 1)$ plane in the case of orientation E when the ε_{cri} reach 0.052.

To reveal the mechanism of fatigue crack extension of various orientations, the cyclic loading was applied with a strain-controlled mode and a load ratio of $R = \varepsilon_{min}/\varepsilon_{max} = 0.8$. The strain rate of cyclic loading is about $1.5 \times 10^9\ s^{-1}$. The values of the maximum strain ε_{max} applied on the specimens of various orientations are shown in Table 4. All atom velocities were generated using a random number generator with the specified seed as temperature 100 K. It is not feasible to study fatigue damage at very low strain rates in molecular dynamics simulation due to the computational cost.

Fig. 5 shows the results of orientation A. The fatigue crack grew on the $(1\ \bar{2}\ 1\ 0)$ plane and propagated along the $[1\ 0\ \bar{1}\ 0]$ direction. The observation plane is the basal plane $(0\ 0\ 0\ 1)$. Three prismatic slip systems $\langle\bar{2}\ 1\ 1\ 0\rangle\{1\ 0\ \bar{1}\ 0\}$ were activated at the crack tip due to the stress concentration. The dislocations emitted from the crack tips move quickly along three $\langle\bar{2}1\ 1\ 0\rangle$ directions. Thus, the crack was significantly blunted and the stress concentration at the crack tips relaxes since 2nd cycle due to the intense dislocation emissions. After growing a very short distance, the fatigue crack stopped growing at 5th cycle.

In the case of orientation B, shown in Fig. 6, the crack on the $(1\ 0\ \bar{1}\ 0)$ plane propagated along the direction of $[1\ \bar{2}\ 1\ 0]$. The view plane also is the basal plane $(0\ 0\ 0\ 1)$. The intense plastic blunting

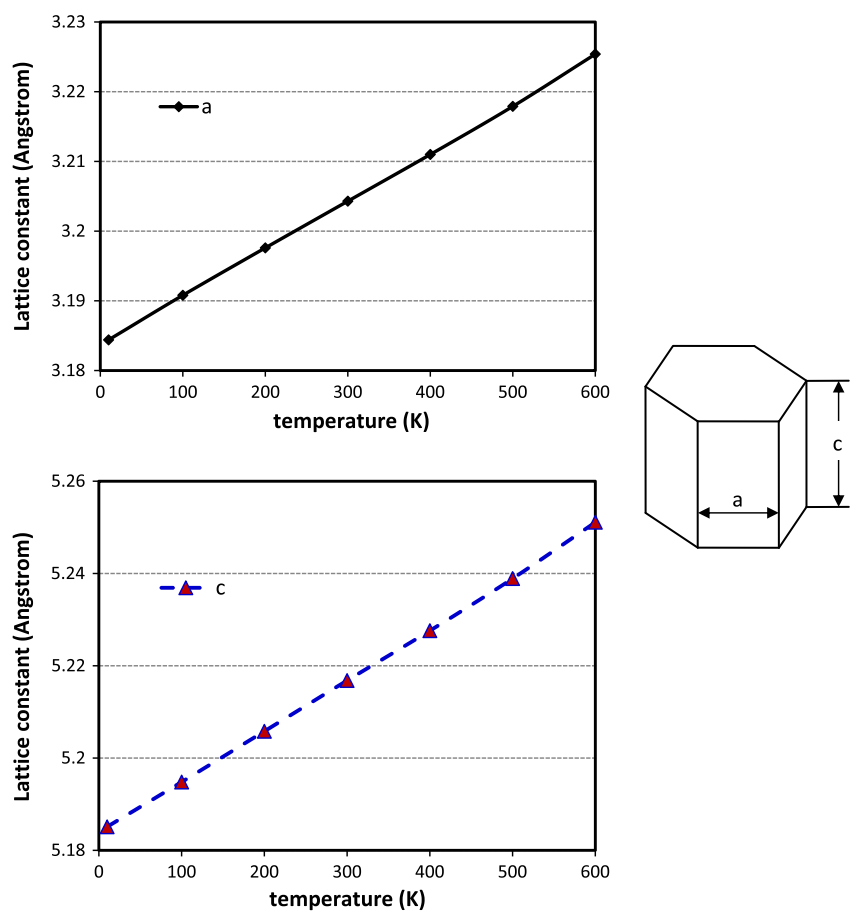

Fig. 4. Variation of lattice constants of magnesium crystal with temperature.

Table 3
The critical values of maximum tension strains ε_{cri} for orientation A–J.

Orientation	A	B	C	D	E	F	G	H	I	J
ε_{cri}	0.055	–	0.046	0.046	0.052	0.041	0.066	0.0435	0.05	0.055

Table 4
The applied maximum tension strains ε_{max} for orientation A–J.

Orientation	A	B	C	D	E	F	G	H	I	J
ε_{max}	0.045	0.045	0.0418	0.0418	0.0425	0.038	0.06	0.0425	0.045	0.05

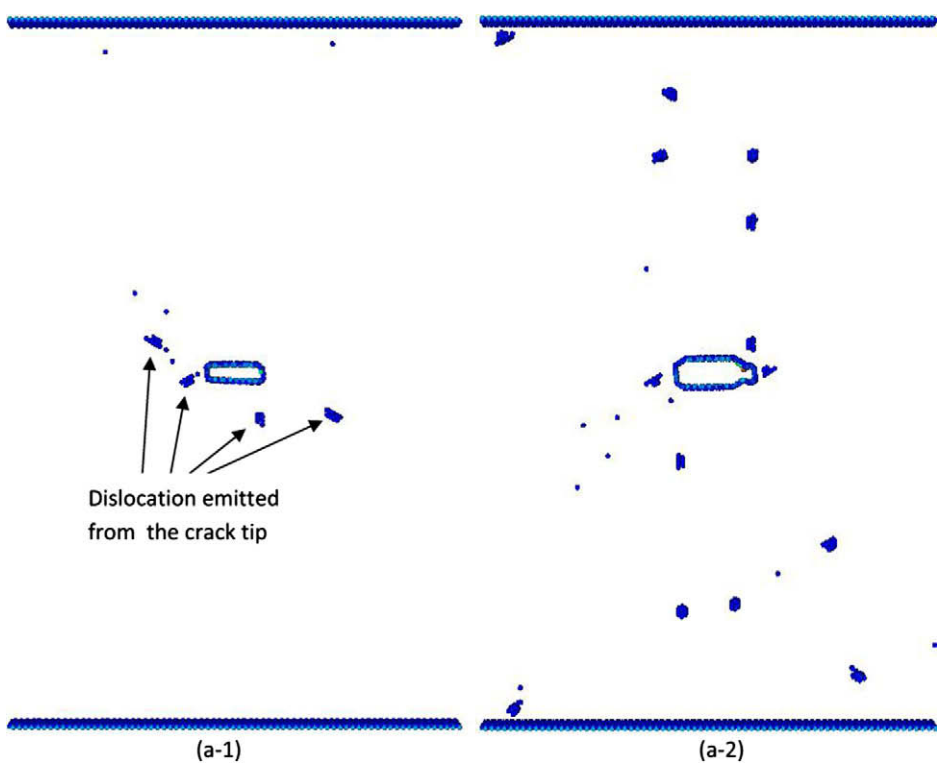

Fig. 5. Simulation of fatigue crack growth in single magnesium crystal of orientation A: (a-1) 1st cycle; (a-2) 5th cycle. Significant dislocation emission from the crack tips can be observed.

occurring at the crack tips results from the dislocation emission caused by the activation of two prismatic slip systems $\langle\bar{2}\,1\,1\,0\rangle\{1\,0\,\bar{1}\,0\}$. The crack was significantly blunted and stopped growing after a small amount of crack extension since the first cycle.

Fig. 7 shows the simulation results from orientation C with the crack in the $(1\,0\,\bar{1}\,0)$ plane and propagation in the $[0\,0\,0\,1]$ direction. There are three possible crack propagation directions: one basal and two pyramidal slip directions. The basal slip direction is excluded for crack propagation direction because resolved tensile stress to open two basal planes is zero in this system. The fatigue crack propagated along a zig-zag path alternating two pyramidal slip directions. Basal and pyramidal slip dislocations are available in this system. Only basal slip dislocations are observed because Peierls stress of basal slip dislocation is much less than one of pyramidal dislocations. This phenomenon is in agreement with the experiment results of Naomi et al. [18]. These slip bands are stacking faults with FCC structures caused by basal slip. Almost no blunting was observed at the crack tip and the cracks grew by fatigue cleavage of atoms in the crack plane. The crack propagated quickly in the crack planes and reached the edge only in three cycles.

In the case of orientation D, shown in Fig. 8, the crack grew straight along the $[0\,0\,0\,1]$ direction in the $(1\,\bar{2}\,1\,0)$ plane which is normal to loading direction. Similar to the case of orientation C, only basal slip dislocations occurred at the crack normal to the direction of the crack propagation. The crack grew very rapidly in the crack planes and reached the edge only in three cycles. The crack tips were not significantly blunted and propagated as the manner of atomic cleavage because there are no other possible layers which have similar resolved tensile stress to open.

Figs. 9 and 10 show the contour plots of σ_y of orientation C and D at second cycle, respectively. Clearly, the stress concentration occurs at the crack tip and results in atomic cleavage at the crack tips.

Fig. 11 shows the results of orientation E with the initial crack in the $(0\,0\,0\,1)$ plane and the crack growth direction along $[1\,0\,\bar{1}\,0]$. The fatigue crack was blunted due to the formation of pyramidal slip band on the $(1\,0\,\bar{1}\,1)$ plane. Starting at 3rd cycle, the fatigue crack grew along pyramidal slip plane. Even though the basal plane normal to loading direction is available which have high tensile

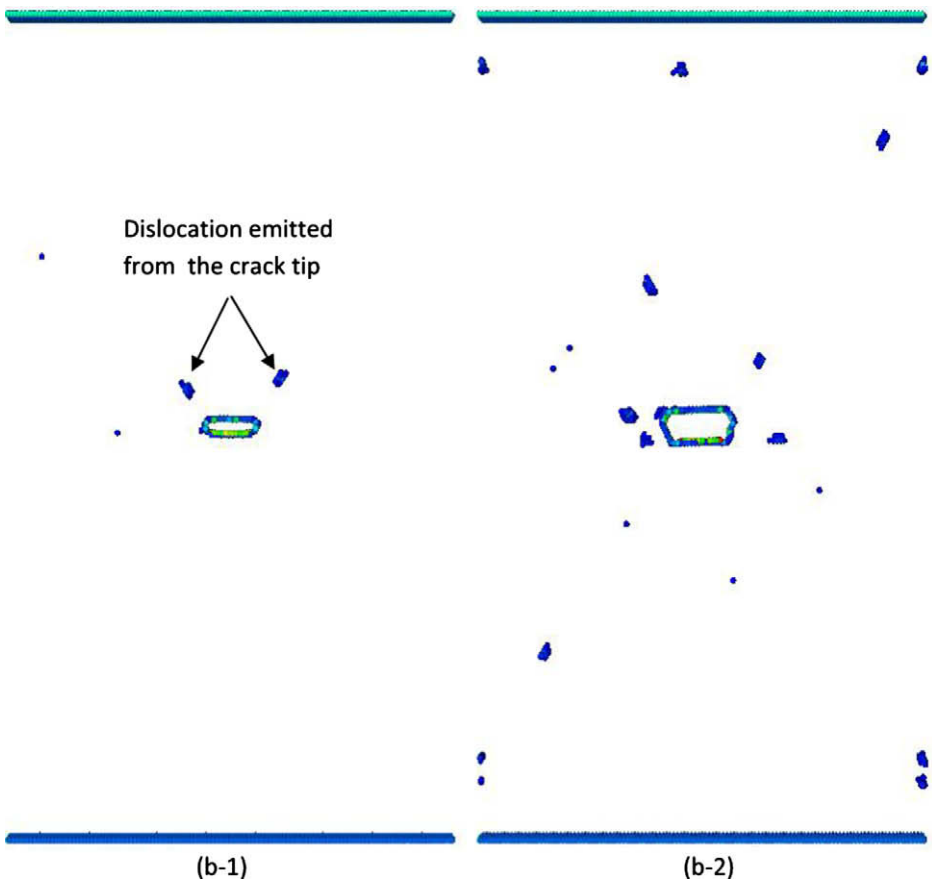

Fig. 6. Simulation of fatigue crack growth in single magnesium crystal of orientation B: (b-1) 1st cycle; (b-2) 5th cycle. Significant dislocation emission from the crack tips can be observed.

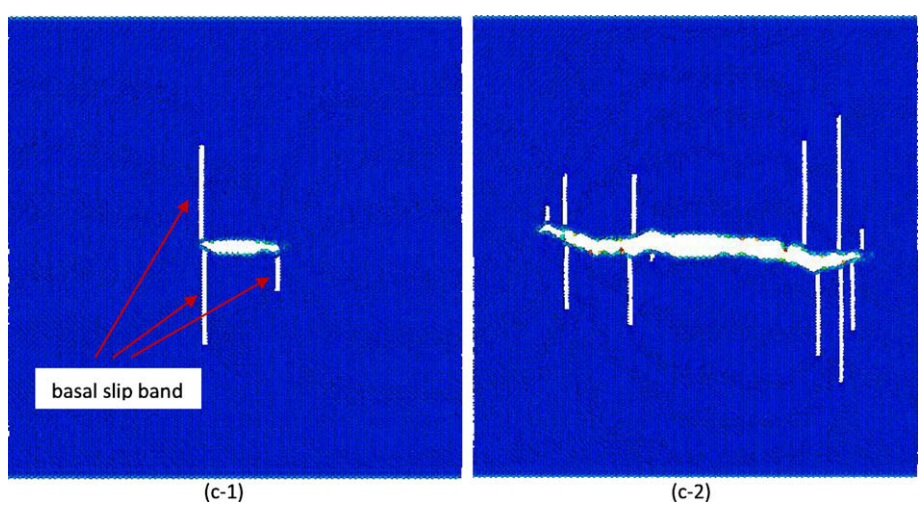

Fig. 7. Simulation of fatigue crack growth in single magnesium crystal of orientation C. (a) 1st cycle; (b) 3rd cycle.

stress, pyramidal planes of low resolved tensile stress are selected for crack to grow on because the pyramidal slip bands sharpen the crack tip and the tensile binding of pyramidal planes is weaker than one of basal planes. The basal dislocations are inactive in this system because the resolved shear stress is zero.

Fig. 12 shows the orientation F of the model with the initial crack in the (0 0 0 1) plane and the crack growth direction along $[1\,\bar{2}\,1\,0]$. The fatigue crack in orientation F propagated stably in the plane (0 0 0 1) along the direction of $[1\,\bar{2}\,1\,0]$. The basal dislocations are inactive in this system because the resolved shear stress is zero. The prismatic and pyramidal slips are suppressed by boundary conditions. Only twinning deformation is available. The $\{1\,1\,\bar{2}\,1\}[\bar{1}\,\bar{1}\,2\,6]$ twin bands were developed at the crack tip since the first cycle due to the stress concentration. In this case,

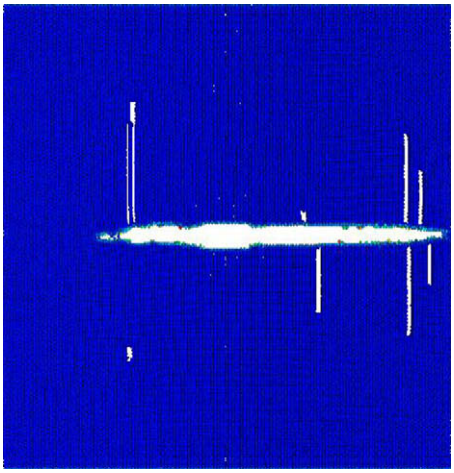

Fig. 8. Simulation of fatigue crack growth in single magnesium crystal of orientation D. (a) 1st cycle; (b) 3rd cycle.

the fatigue crack grew slowly due to the formation of the twin bands which moved with the crack tip. Fig. 12(f-2) shows the atomic structure of the $\{1\ 1\bar{2}\ 1\}[\bar{1}\ \bar{1}\ 2\ 6]$ twin bands occurring at the crack tips.

Fig. 13 shows the results in the case of orientation G with the crack in the $(1\ 0\ \bar{1}\ 1)$ plane and the propagation direction of $[1\ \bar{2}\ 1\ 0]$. Since the first cycle, the dislocation emission from the crack tip corresponding to the slip plane $(2\ 0\ \bar{2}\ 1)$ were observed. The basal and pyramidal slips are suppressed by boundary conditions and only prismatic slips are active. The fatigue crack started growing since 3rd cycle. Once the fatigue crack start growing, it grew rapidly and reached the edge in another one cycle because a pyramidal plane is normal to loading direction and layer-to-layer distance is large.

Fig. 14 shows the results from the orientation H. The crack grew in the $(1\ 0\ \bar{1}\ 1)$ plane and the propagation direction along the direction of $[\bar{1}\ 0\ 1\ 2]$. Basal slip bands were observed at the crack tips. The crack grew very rapidly and reached the edge in three cycles because one of pyramidal plane is normal to loading direction and their layer-to-layer distance is wide and easy to open. The large resolved shear stress and low Peierls stress of basal slip system prevent the activation of the other slip systems such as pyramidal slip systems.

The simulation results of orientation I were shown in Fig. 15 with the crack in the $(1\ 0\ \bar{1}\ 2)$ and propagation along the $[1\ \bar{2}\ 1\ 0]$ direction. At 3rd cycle, pyramidal slip bands occur at the crack tips. Starting at cycle 5, the right crack tip propagated along the right pyramidal slip band with mixed Mode I + Mode II. The left crack tip grew on the twin slip plane. The anisotropy of slip band nucleation comes from geometrical anisotropy.

Fig. 16 shows the results of orientation J. In this case, the crack grew on the $(1\ 0\ \bar{1}\ 2)$ plane with zig-zag path and along the direction of $[\bar{1}\ 0\ 1\ 1]$. The basal and pyramidal slip dislocation emission occurred from the crack tips during cyclic loading. There is not much crack tip blunting because of not much dislocation emission. The layer-to-layer distance in basal and pyramidal planes are wide so cracks grow in alternating three directions and form a zig-zag path.

To show the fatigue damage caused by persistent slip band in orientation E and fatigue crack propagation in orientation B, we used CC specimen applied by the increased maximum strain cyclic loading as indicated in Fig. 17 along y direction and the periodic boundary condition is assigned along x and z direction. Fig. 18 shows the fatigue crack propagation process. Significant crack blunting was observed since 2nd cycle due to the plastic slip along two slip bands corresponding to the directions $[\bar{1}\ 0\ 1\ 2]$ and $[\bar{1}\ 0\ 1\ \bar{2}]$ and the crack did not grow along the direction $[\bar{1}\ 0\ \bar{1}\ 0]$. The fatigue crack propagated along the primary slip band with mixed Mode I + II since 5th cycle. Since cycle 12, the crack grew

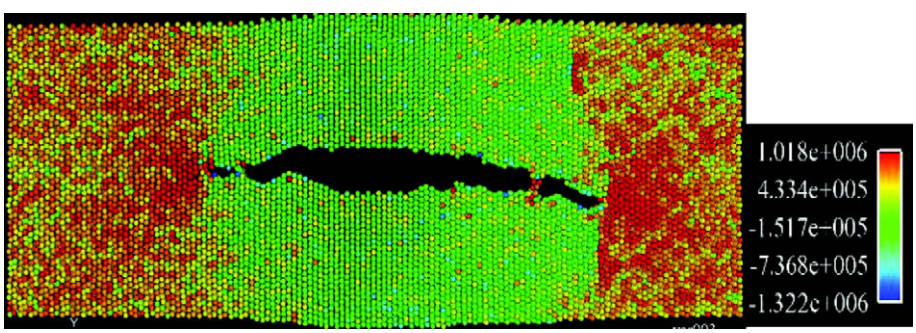

Fig. 9. Contour plot of stress σ_y (bar) in Orientation C at 2nd cycle.

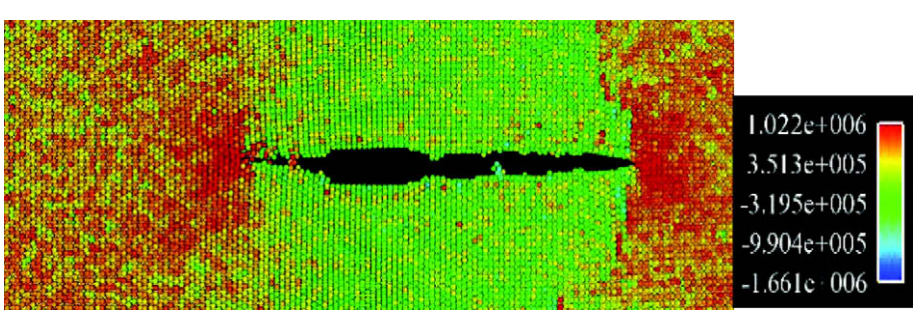

Fig. 10. Contour plot of stress σ_y (bar) in Orientation D at 2th cycle.

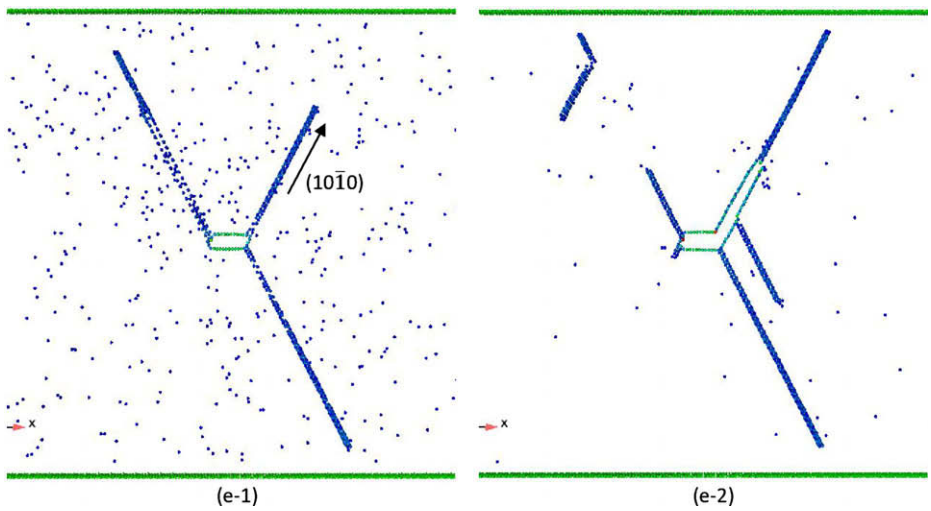

Fig. 11. Simulation of fatigue crack growth in single magnesium crystal in orientation E. (e-1) 2nd cycle; (e-2) 3rd cycle. Slip bands were developed along (10$\bar{1}$1) plane at crack tip in orientation E.

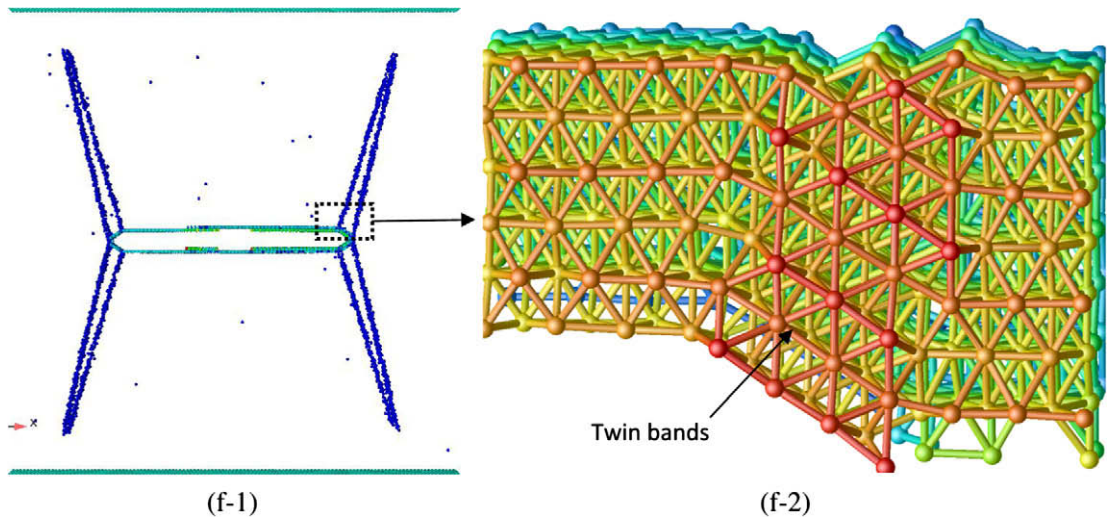

Fig. 12. Simulation of fatigue crack growth in single magnesium crystal in orientation F. (f-1) 4th cycle; (f-2) atomic structure of {1 1 $\bar{2}$ 1}[$\bar{1}$ $\bar{1}$ 2 6] twin bands at the crack tips.

alternatively along the slip bands in the planes [$\bar{1}$ 0 1 2] and [0 0 0 1], respectively. Fig. 19 shows the contour plot of fatigue crack in orientation B at 14th cycle. It can be seen that the crack tip was significantly blunted and deformed to round shape under the application of high value of tension strain. Some voids nucleated in the matrix due to the combination of emitted dislocations.

Based on the above simulation results, it is evident that different orientations present different mechanism of crack extension. The plastic deformation mode at the crack tips is the major influencing factor to fatigue crack propagation. It either blunted the crack or enhanced the fatigue crack extension. Another feature of fatigue crack growth is that even though the crystal structures and loading are symmetric, the Brownian random motion of atoms in molecular dynamic simulations causes non-symmetric crack growth, such as in the cases of orientation A–F. The grow rate and propagation path of fatigue crack vary widely from one orientation to another. To better quantify the crack growth rate of different orientation, we simulated the fatigue crack growth in different crystal orientation using EC specimen. The cyclic loading is the same as those applied to CC specimen, namely, the maximum strain $\varepsilon_{max} = 4.25 \times 10^{-2}$ and a load ratio of $R = \varepsilon_{min}/\varepsilon_{max} = 0.75$. Note that, undoubtedly, we can also use CC specimens to calculate the crack growth rate. In the previous studies on atomistic modeling of fatigue behavior in FCC crystals [8–10], the EC specimens were not employed. Therefore, we want to try using EC specimens in the present study. The simulation results from EC specimens show the same mechanism of fatigue crack growth as those from CC specimens. The model temperature at which the simulations were carried out was a constant temperature of 10 K. Fig. 20 shows the comparison of variation of crack length with the number of cycles for different orientation. The results of orientation B and E are close to that of orientation A so that only the results of orientation A are plotted. The comparison results clearly indicated that the mechanism of fatigue crack propagation is strongly dependent on the crystal orientation of the initial crack. The crack growth rate of orientation D is the highest. The crack propagated with stable growth rate in orientation D and F. In the simulations of EC specimen, no crack growing occurred in the orientation G.

Normally, the strain rate has little effects of fatigue damage when its value is low. However, at high value of strain rate, the

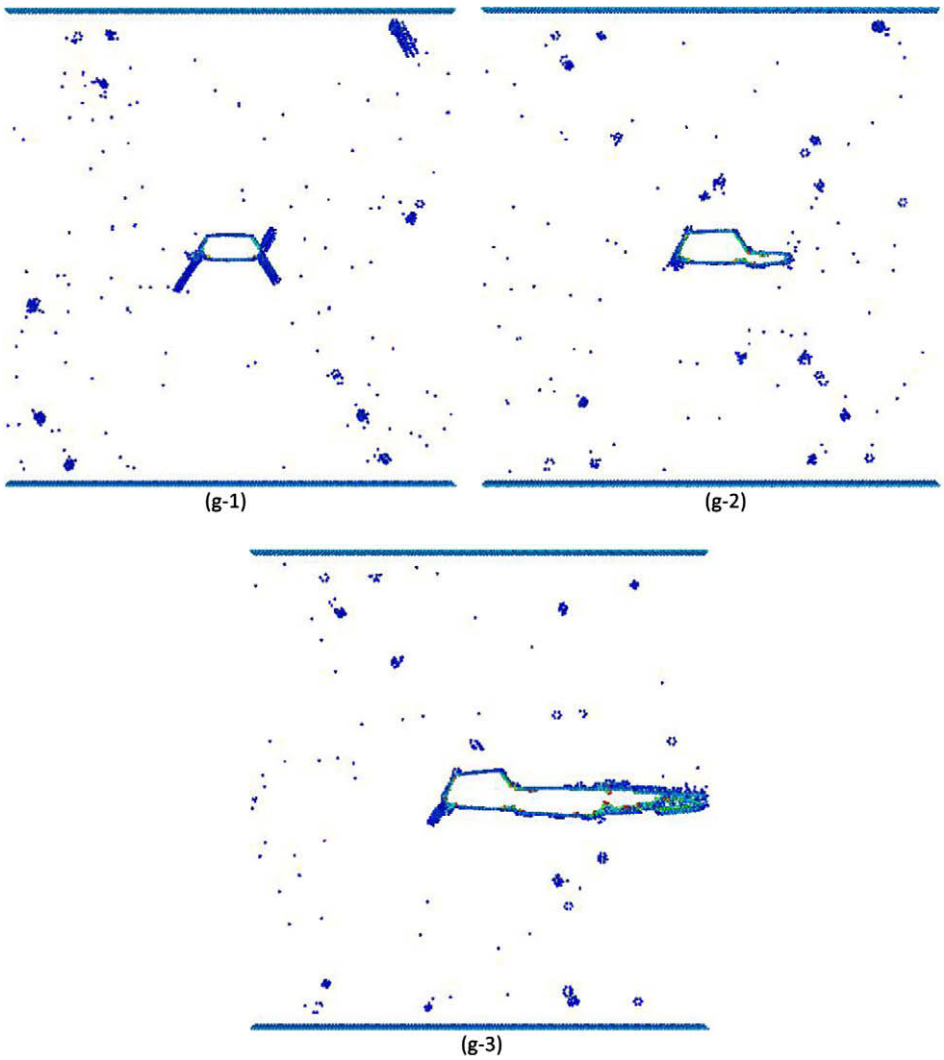

Fig. 13. Simulation of fatigue crack growth in single magnesium crystal for orientation G. (g-1) 1st cycle; (g-2) 3rd cycle; (g-3) 4th cycle.

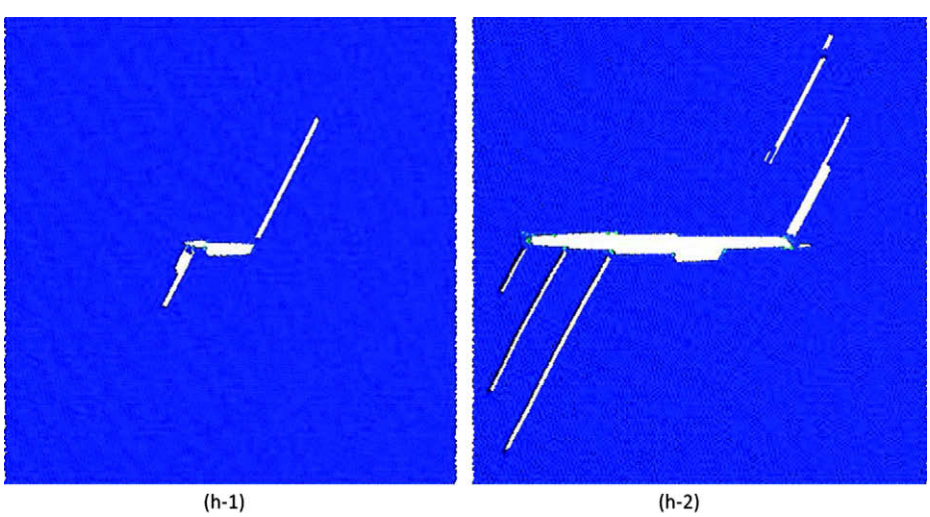

Fig. 14. Simulation of fatigue crack growth in single magnesium crystal for orientation H: (h-1) 1st cycle; (h-2) 3rd cycle.

loading frequency will affect the fatigue crack growth in our simulation on magnesium. The effects of strain rate on the crack growth rate were investigated on the specimen of orientation F. The comparison results obtained from various strain rates are presented in Fig. 21. Clearly, the growth rate decreases with strain rate increasing.

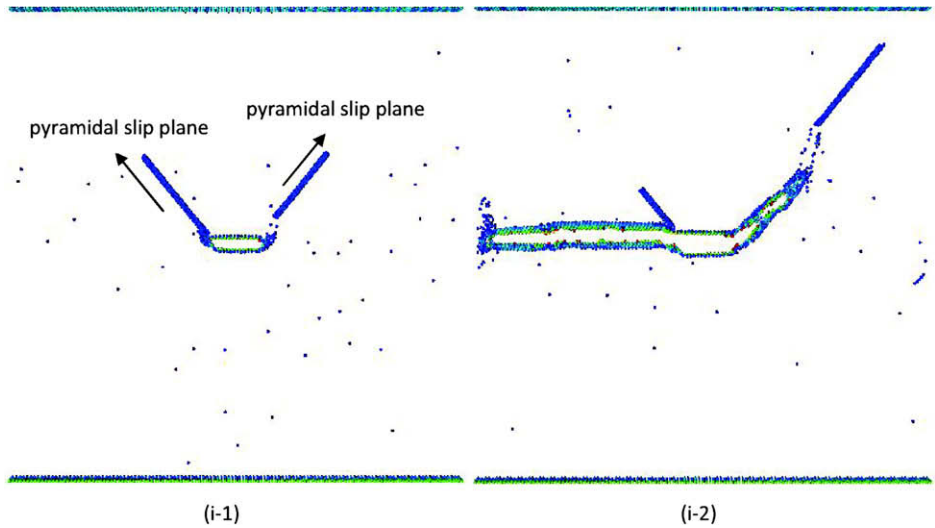

Fig. 15. Simulation of fatigue crack growth in single magnesium crystal in orientation I. (i-1) 3rd cycle; (i-2) 5th cycle.

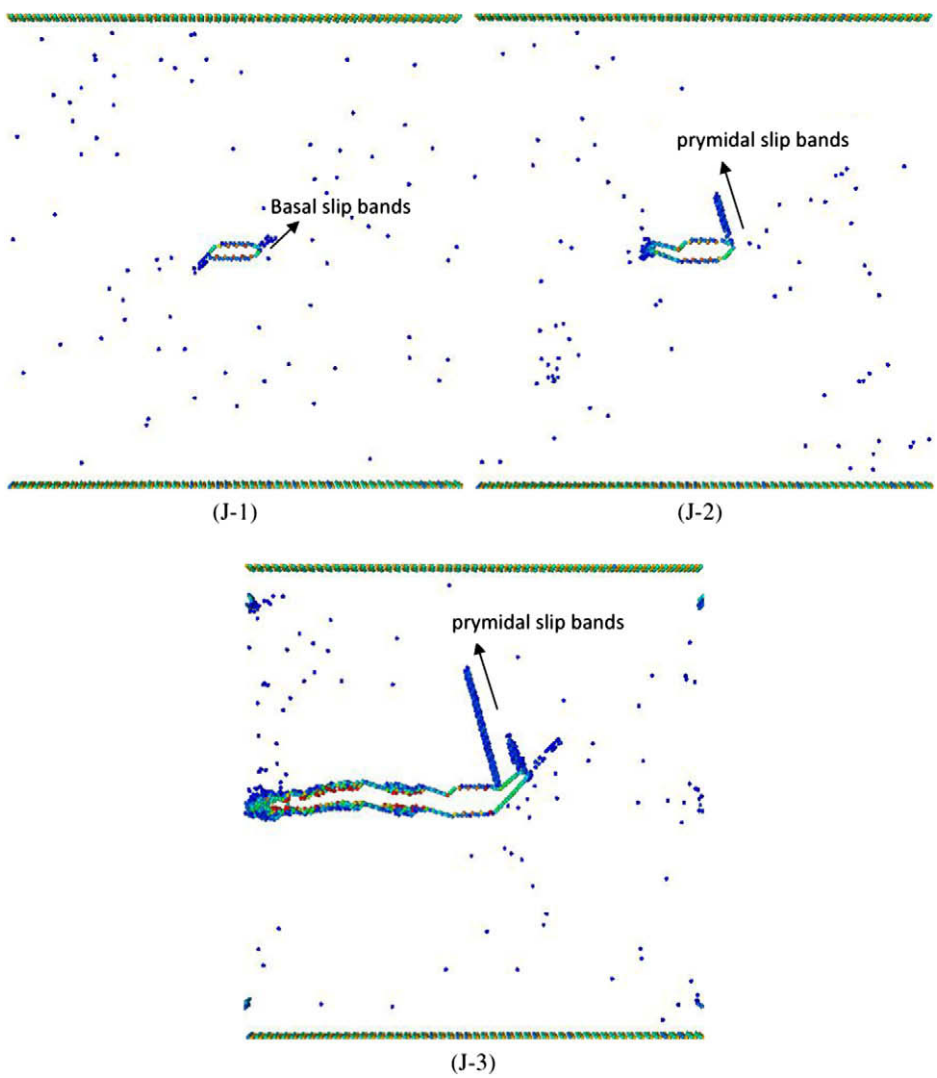

Fig. 16. Simulation of fatigue crack growth in single magnesium crystal in orientation J: (J-1) 1st cycle; (J-2) 2nd cycle; (J-2) 4th cycle.

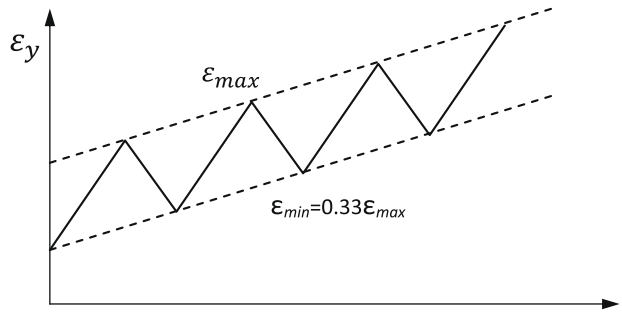

Fig. 17. Increased maximum strain cyclic loading used for the simulation of fatigue damage caused by slip band in orientation E.

5.2. Effects of temperature

In this section, the study is focus on the temperature effects on the mechanism of fatigue crack propagation of different orientation of initial crack. The simulations were performed at various temperatures, namely, 10 K, 100 K, 300 K, and 500 K. To keep the temperature constant, the specimen was firstly equilibrated at desired constant temperature by rescaling the velocities of atoms. Then, the NVT operation was carried out to update the positions and velocities each timestep. V is volume and T is temperature. This creates a system trajectory consistent with the canonical ensemble. For all specimens, the cyclic loading is applied in a strain-controlled mode with the maximum strain level of $\varepsilon_{max} = 0.045$ and the strain ratio of $R = \varepsilon_{min}/\varepsilon_{max} = 0.75$. The strain rate is $4.5 \times 10^9\ s^{-1}$.

The simulation results show that the temperature does not have significant influences on the mechanism of fatigue crack growth of all orientations except orientation A. In the cases of orientations B and E, the fatigue cracks were blunted and stopped growing since the second loading cycle at various temperatures. The contour plots of centrosymmetry number of orientation A at various temperatures at cycle 15 are shown in Fig. 22. At temperature 10 K and 100 K, the fatigue crack stopped growing since the second cycle while at 300 K and 500 K the crack stopped growing since cycle 3 and cycle 13, respectively. The propagation mechanism at high temperature was the nucleation, growth, and coalescence of the voids ahead of the crack tip and the linkage of the void with the main crack as illustrated in Fig. 23. The nucleation of void is due to the stress concentration ahead the crack tip where the materials become soft resulting from high temperature.

The temperature effects on the growth rate of the orientation C, D, F, G, and H are shown in Figs. 24–28, respectively. In general, in these orientations, the growth rate of fatigue crack increased with decreasing temperature. The simulation results imply that the

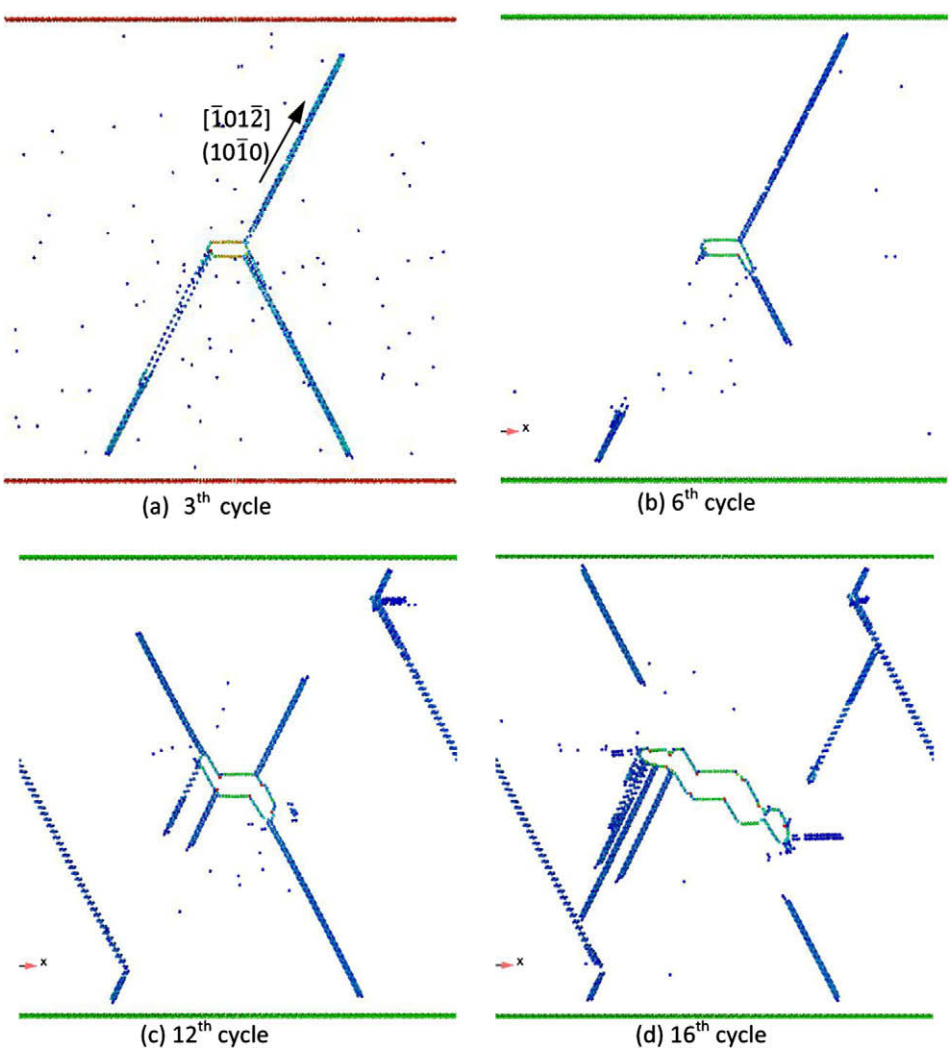

Fig. 18. Simulation of fatigue damage by increased maximum strain cyclic loading in orientation E.

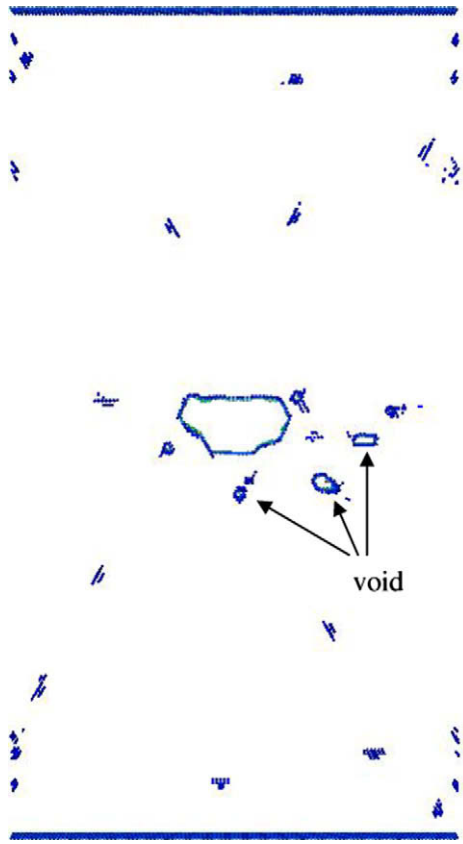

Fig. 19. Simulation of fatigue damage by increased maximum strain cyclic loading in orientation B at 14th cycle.

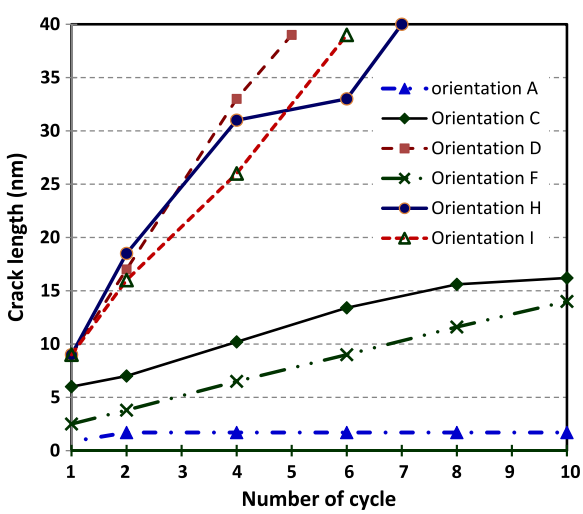

Fig. 20. Variation of crack length with number of cycles for different orientations.

material is getting ductile with increasing temperature and consequently the increased resistance of fatigue crack growth.

6. Conclusions

The fatigue crack growth in magnesium single crystals at nanoscale was investigated using molecular dynamics simulation. Ten

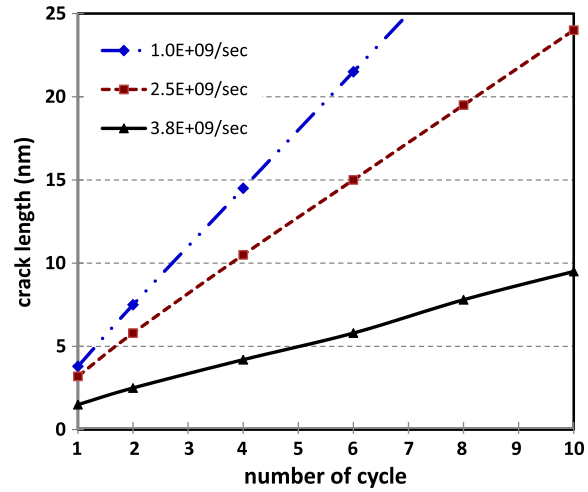

Fig. 21. Influences of strain rate on fatigue crack growth in the specimen of orientation F.

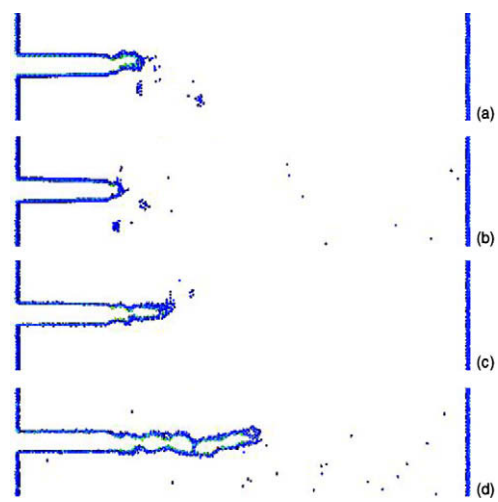

Fig. 22. Centrosymmetry parameter contour plot of specimens of orientation A at various temperatures at cycle 15 (a) 10 K; (b) 100 K; (c) 300 K; (d) 500 K.

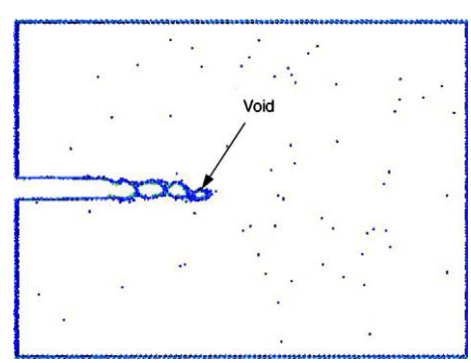

Fig. 23. The mechanism of fatigue crack growth at 500 K is the nucleation of void in front of the crack tip and the linkage back with the main crack.

different initial crack orientations were considered. This study is focus on revealing the mechanism of fatigue crack propagation at various crystal orientations and the temperature effects on the fa-

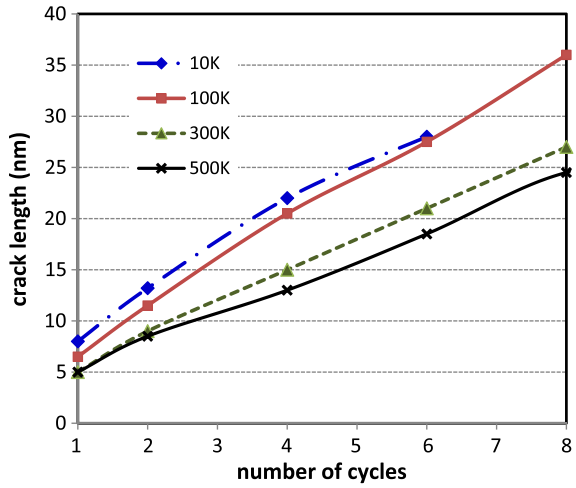

Fig. 24. The variation of crack length with the number of cycles for orientation C at various temperatures.

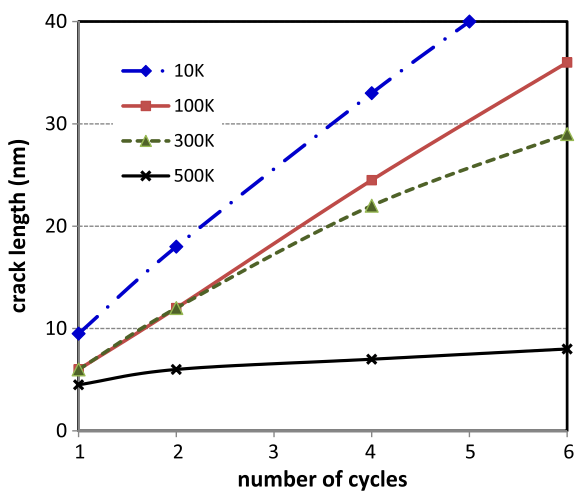

Fig. 25. The variation of crack length with the number of cycles for orientation D at various temperatures.

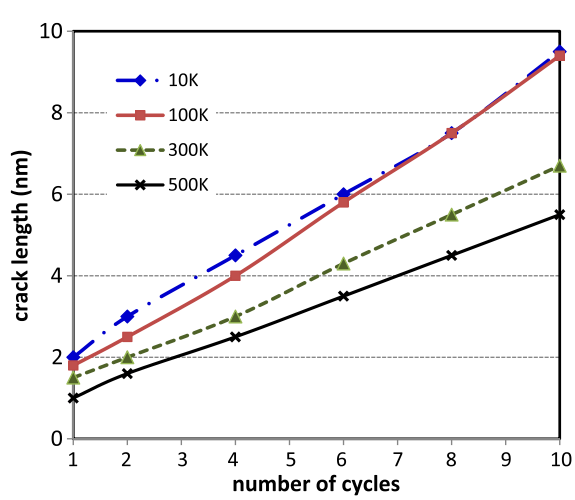

Fig. 26. The variation of crack length with the number of cycles for orientation F at various temperatures.

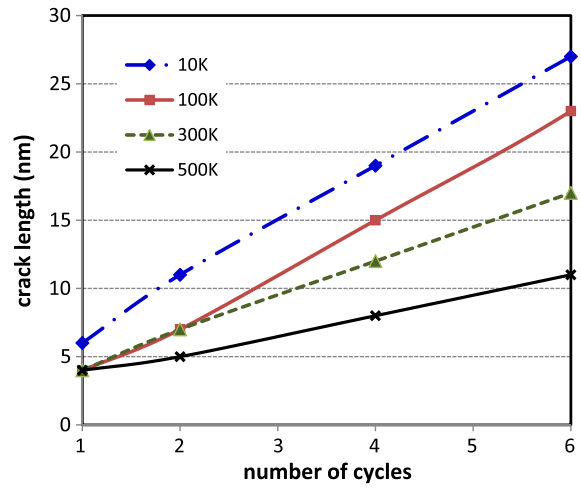

Fig. 27. The variation of crack length with the number of cycles for orientation G at various temperatures.

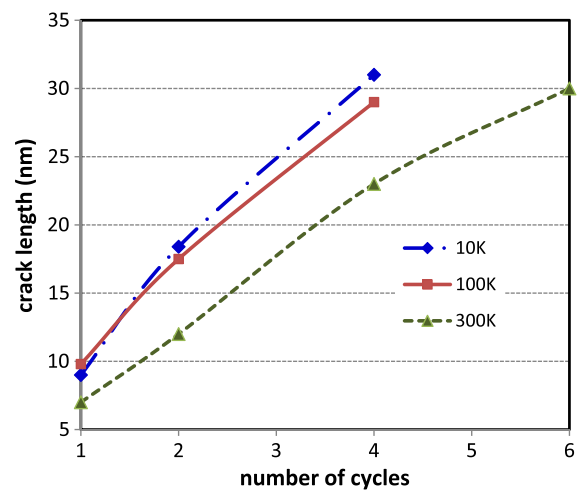

Fig. 28. The variation of crack length with the number of cycles for orientation H at various temperatures. In this case, the fatigue crack does not grow at 500 K.

tigue behavior. The following major conclusions can be drawn according to the simulation results:

1. The mechanism of fatigue crack propagation is strongly dependent on the crystal orientation of the initial crack.
2. The resistance of fatigue crack growth of orientation B is the highest while the crack growth rate of orientation D is the highest.
3. The dislocation emissions and twin bands occurring at the crack tips due to the stress concentration play major roles on the mechanism of fatigue crack growth. The plastic deformation at the crack tip has dual effects on the fatigue crack growth. It can either enhance the fatigue crack growth or increase the resistance to fatigue crack growth.
4. The growth rate of fatigue crack growth decreased with increasing strain rate at the nanoscale.
5. The mechanism of fatigue crack growth in the orientation A was strongly affected by the temperature, while the temperature does not have significant influences on the mechanism of fati-

gue crack extension of other orientations. However, the growth rate decreases with increasing temperature in all orientations except orientation A, B, and E.

Acknowledgement

The authors acknowledge the Center for Advanced Vehicular Systems at Mississippi State University and the Department of Energy for supporting this research.

References

[1] B. Mordike, T. Ebert, Mater. Sci. Eng. A-Struct. 302 (2001) 37.
[2] K. Kainer, Magnesium Alloys and their Applications, Wiley-VCH Verlag GmbH, Weinheim, Germany, 2004.
[3] L. Duffy, Magnesium alloys: the light choice for aerospace, Material World, 1996.
[4] E. Schubert, M. Klassen, I. Zerner, G. Sepold, J. Mater. Process. Technol. 115 (2001) 2.
[5] G. Cole, Mater. Sci. Forum 419–422 (2003) 43.
[6] S. Schumann, H. Friedrich, Mater. Sci. Forum 419–422 (2003) 51.
[7] S. Ando, K. Saruwatari, T. Hori, H. Tonda, J. Jpn. Inst. Metals 67 (2003) 247.
[8] G.P. Potirniche, M.F. Horstemeyer, B. Jelinek, G.J. Wanger, Int. J. Fatigue 27 (2005) 1179.
[9] G.P. Potirniche, M.F. Horstemeyer, Phil. Mag. Lett. 86 (2006) 185.
[10] G.P. Potirniche, M.F. Horstemeyer, P.M. Gullett, B. Jelinek, Proc. Royal Soc. A 462 (2006) 3707.
[11] D. Farkas, M. Willemann, B. Hyde, Phys. Rev. Lett. 94 (2005) 165.
[12] K. Nishimura, N. Miyazaki, Compos. Mater. Sci. 31 (2004) 269.
[13] B. Lim, C. Jeong, Y. Keum, Met. Mater. Int. 9 (2003) 543.
[14] W.-J. Chang, T.-H. Fang, J. Phys. Chem. Solids 64 (2003) 1279.
[15] F. Saghir, N. Merah, Z. Khan, A. Bazoune, J. Mater. Process. Technol. 164–165 (2005) 1550.
[16] D.Y. Sun, M.I. Mendelev, C.A. Becker, K. Kudin, T. Haxhimali, M. Asta, J.J. Hoyt, Phys. Rev. B 73 (2006) 024116.
[17] C. Kelchner, S. Plimpton, J. Hamilton, Phys. Rev. B 58 (1998) 11085.
[18] L. Naomi, A. Shinji, T. Masayuki, K. Hiromoto, T. Hideki, Key Eng. Mater. 345–346 (2007) 307.